CHEMISTRY OF MATERIALS
Cite This: Chem. Mater. 2019, 31, 6962–6970
Article
pubs.acs.org/cm

Organic Semiconductors Derived from Dinaphtho-Fused *s*-Indacenes: How Molecular Structure and Film Morphology Influence Thin-Film Transistor Performance

Andrew M. Zeidell,[†] Laura Jennings,[†] Conerd K. Frederickson,[‡] Qianxiang Ai,[§] Justin J. Dressler,[‡] Lev N. Zakharov,[∥] Chad Risko,[§] Michael M. Haley,[‡] and Oana D. Jurchescu*[,†]

[†]Department of Physics and Center for Functional Materials, Wake Forest University, Winston-Salem, North Carolina 27109, United States

[‡]Department of Chemistry & Biochemistry and the Materials Science Institute, University of Oregon, Eugene, Oregon 97403-1253, United States

[§]Department of Chemistry and Center for Applied Energy Research (CAER), University of Kentucky, Lexington, Kentucky 40506, United States

[∥]CAMCOR—Center for Advanced Materials Characterization in Oregon, University of Oregon, Eugene, Oregon 97403-1433, United States

Supporting Information

ABSTRACT: Charge-carrier transport in thin-film organic semiconductors is strongly related to the molecular structure and the solid-state packing, which in turn are dependent on materials processing and device configurations. We report on the synthesis and characterization of a series of (trialkylsilyl)ethynyl-substituted dinaphtho-fused *s*-indacenes that include three regioisomers: the *linear*, *syn*, and *anti* isomers. Structure–property relationships are established for these antiaromatic compounds by combining X-ray diffraction with field-effect transistor measurements and density functional theory (DFT) evaluations of the electronic band structures and intermolecular electronic couplings. High-performance, solution-processed organic thin-film transistors with charge-carrier mobilities over 7 $cm^2/(V\ s)$ are demonstrated upon optimization of the thin-film morphology. The DFT-derived crystal band structures provide insight into the varied performance metrics observed across the materials, though the fundamental limits of performance are not reached when the film quality is poor. The totality of the results presents the antiaromatic dinaphtho-fused *s*-indacenes as intriguing building blocks for molecular materials for semiconducting applications.

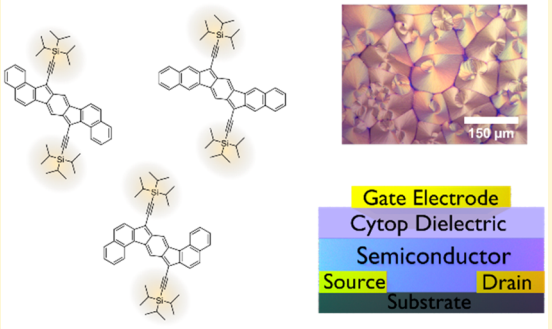

INTRODUCTION

Organic semiconductors have maintained broad academic and industrial attention due to their distinctive optoelectronic properties and the applications they can enable. Such devices are obtained by unconventional manufacturing such as spray coating,[1] inkjet printing,[2,3] or laser printing[4] - low-cost processes occurring in mild conditions, which may enable new device functionalities that are either impossible or not cost-effective with current technologies (lightweight, mechanical flexibility, conformability, and transparency, etc.). The ability to control the properties through chemical design provides a versatile tool for the development of materials with specific function in mind, but unfortunately this task is challenged by the intricate relationships among the molecular structure, processing, film morphologies (molecular to mesoscale), and ultimate materials performance in device applications.

Molecular materials built from polycyclic aromatic hydrocarbons, such as pentacene, tetracene, or rubrene, have served as excellent model systems to explore structure–function relationships of organic semiconductors, given their simple structure.[5−8] Functionalization of the backbone has allowed for enhanced environmental stability and film deposition using solution-based methods,[9] which are key properties for their incorporation in low-cost, large-area flexible electronic devices. Nevertheless, these substituted oligoacenes still suffer from stability issues in the case of longer backbones, where dimerization and/or photooxidation frequently occur under ambient conditions.[10−12] The reduced aromaticity obtained by replacing two six-membered rings with five-membered

Special Issue: Jean-Luc Bredas Festschrift

Received: April 11, 2019
Revised: May 16, 2019
Published: May 22, 2019

DOI: 10.1021/acs.chemmater.9b01436
Chem. Mater. 2019, 31, 6962–6970

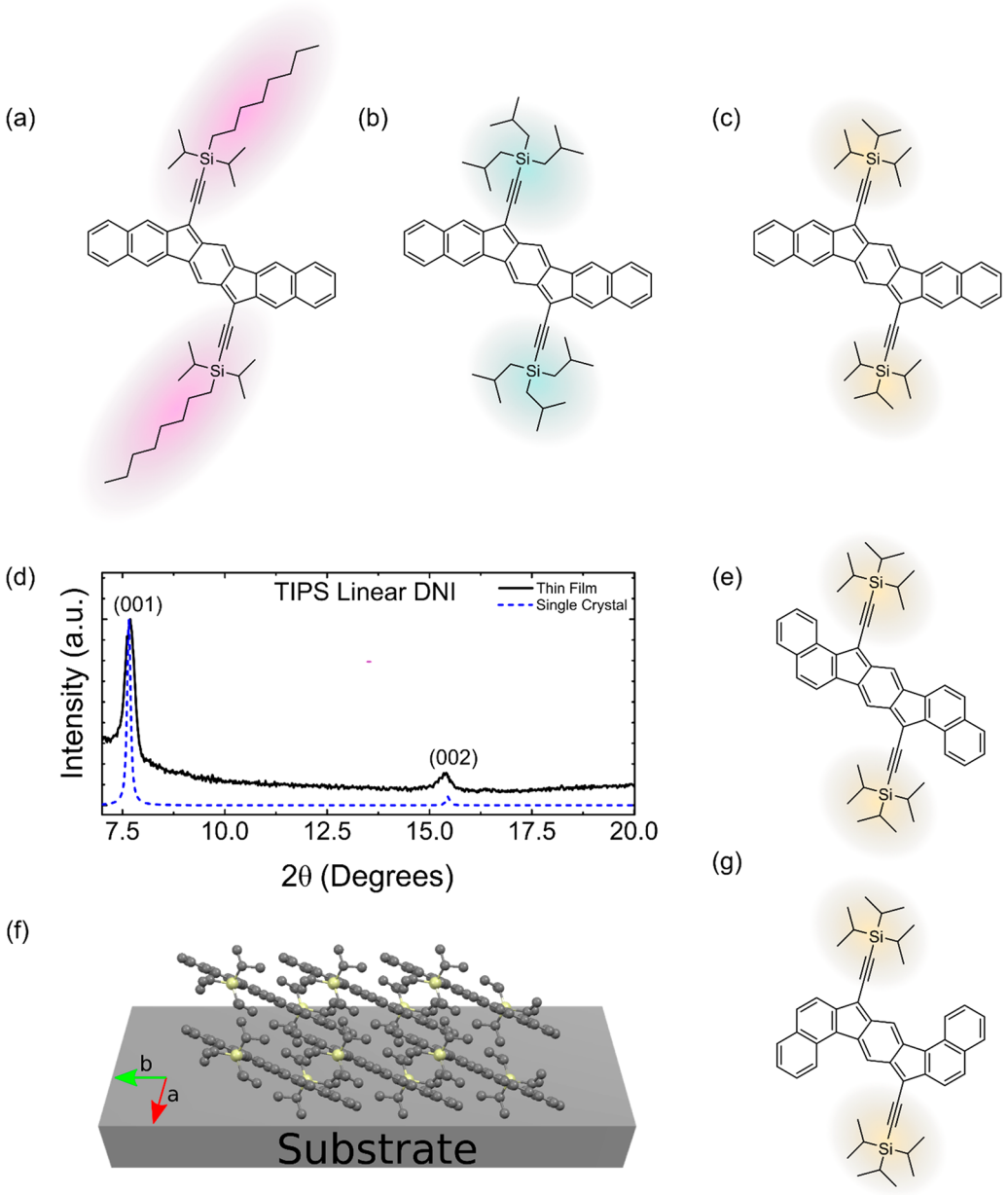

Figure 1. Chemical structures of the dinaphthoindacene isomers and substituent groups used in this study: (a) nODIPS *linear* DNI, (b) TIBS *linear* DNI, (c) TIPS *linear* DNI, (d) 2θ XRD of a TIPS *linear* DNI film on SiO_2, (e) TIPS *anti* DNI, (f) illustration of TIPS *linear* DNI packing, with the substrate lying in the (001) plane, and (g) TIPS *syn* DNI.

heterocyclic rings led to better stability and more efficient charge transport in heteroacenes, such as dithiophenes and dibenzothienothiophenes.[13−15] Molecules containing indolizine or diindolizine heterocyclic aromatic units were also developed and tested in devices.[16,17] Such structural modifications have led to systems with charge-carrier mobilities as high as 20 $cm^2/(V\ s)$ obtained in difluoro(triethylsilylethynyl)anthradithiophene[18] and with 2,7-dioctyl[1]benzothieno[3,2-*b*][1]benzothiophene (C8-BTBT) exhibiting charge-carrier mobilities as high as 30 $cm^2/(V\ s)$.[19]

Antiaromatic molecules such as pentalene and indacene are conjugated cyclic hydrocarbons containing destabilized $4n$ π-electrons;[20] for reference, aromatic compounds have $(4n + 2)$ π-electrons. An inherent destabilization due to the antiaromatic character results in a small energy gap between the highest occupied molecular orbital (HOMO) and the lowest unoccupied molecular orbital (LUMO),[21] low-lying HOMO and LUMO energy levels, and pronounced bond length alternation compared to aromatic compounds.[22] Antiaromatic compounds tend to be unstable, but including them within larger conjugated systems (e.g., dibenzopentalenes and indenofluorenes) can overcome this issue.[22−27] Such compounds have recently been considered for use in semiconducting materials, with studies reported for dibenzopentalenes, dinaphthopentalene, and dianthracenopentalene derivatives,[27−29] as well as for indenofluorene[30] and indacenodibenzothiophene[24] systems. Preliminary results pointed to mobilities on the order of 0.01−0.1 $cm^2/(V\ s)$, with mobilities as high as 0.44 $cm^2/(V\ s)$ for the indacenodibenzothiophenes[24] and as high as 0.52 $cm^2/(V\ s)$ for benzodicyclobutadiene derivatives.[31] Very recent studies have shown it is possible for organic field-effect transistors

DOI: 10.1021/acs.chemmater.9b01436
Chem. Mater. 2019, 31, 6962−6970

(OFETs) with antiaromatic molecules in the active layer to surpass 1 $cm^2/(V\ s)$, with cyclobutadiene-containing systems possessing values as high as 2.9 $cm^2/(V\ s)$.[32]

Developing stable organic semiconductors for high-performance, reliable, and robust devices is not a trivial task given the different factors that should be considered and, that sometimes, are conflicting. To enable a rational design of new molecular structures, it is imperative that we build a well-informed picture of the relationship between the molecular structure, solid-state packing, film morphology in relation with processing, and, ultimately the electrical properties. In this study, we synthesized a series of dinaphtho-fused *s*-indacenes,[25] systematically modified the chemical structure, and evaluated their electronic and electrical properties using a combined experimental and computational approach. Three different substitutions of the *linear*-fused dinaphtho-*s*-indacene (DNI) backbone were investigated, namely, (*n*-octyldiisopropylsilyl)ethynyl (nODIPS), (triisobutylsilyl)-ethynyl (TIBS), and (triisopropylsilyl)ethynyl (TIPS), as shown in Figure 1a–c. In addition to the *linear*-fused DNI, TIPS substituted *anti* and *syn* (Figure 1e,g) regiosomers were also studied. Film morphologies were altered by solvent vapor annealing (SVA) and the electrical properties of the DNIs were evaluated in OFETs. We found that the subtle variations in the side-group chemistry and dinaphthoindacene framework led to significant changes in molecular packing and therefore electrical properties. The best performance was measured in the TIPS *anti*-isomer, which exhibited charge-carrier mobilities as high as 7.1 $cm^2/(V\ s)$, in agreement with characteristics derived from periodic density functional theory (DFT) evaluations of the electronic properties of the bulk crystal.

EXPERIMENTAL SECTION

Molecule Preparation. The three TIPS DNI regioisomers along with the TIBS DNI were prepared as previously described.[25,33] The nODIPS DNI compound was synthesized in an analogous manner, the details of which are in the Supporting Information and Figure S1.

Device Fabrication. Top-gate, bottom-contact OFETs were fabricated on SiO_2 substrates following procedures described elsewhere.[18] Different solvents were tested for film deposition and postprocessing (acetone, hexane, toluene, chlorobenzene, and 1,2-dichlorobenzene), and the results obtained on the best quality films are included in this work. For TIPS *linear* DNI devices, a 1 wt % solution in room-temperature chlorobenzene was spin coated onto this substrate, with predefined source and drain electrodes (Ag and Au were tested; Ag yielded the best results). The as-cast film was subsequently solvent annealed in chlorobenzene vapor at 75 °C for 1 h in a Petri dish. For TIPS *anti* DNI devices, Au contacts were most effective. Here, a 1 wt % solution in room-temperature 1,2-dichlorobenzene was spin coated onto the substrate. For all devices, undiluted Cytop fluoropolymer was used as a gate dielectric, which was spin coated over the organic semiconductor. The dielectric thickness was 1400 nm.[34] The devices were subsequently annealed at 110 °C for 1 h in a vacuum oven to cross-link the dielectric layer and left to cool overnight. A 60 nm Au gate electrode was patterned through a shadow mask aligned over the conduction channel using thermal evaporation. Details on other deposition methods for the films, such as drop cast and solvent assisted crystallization (SAC), are included in the Supporting Information (SI).[35]

Device Characterization. OFETs were measured immediately after fabrication under ambient conditions using an Agilent 4156 semiconductor analyzer. The field-effect mobility (μ) was determined from the saturation regime, using an applied drain-source voltage of V_{DS} = −60 V, by standard procedures.[36] The average values are obtained from at least 30 devices obtained from a minimum of five different substrates.

X-ray Diffraction. *Single-Crystal XRD.* Single crystals of the nODIPS DNI and TIBS DNI were grown via slow diffusion of acetonitrile into deuterochloroform at −40 °C; see the SI for full details. The crystal structures of the TIPS DNI isomers have been disclosed previously.[24]

Thin-Film XRD. 2θ scans of TIPS *linear* DNI deposited onto SiO_2 were obtained using an X-ray diffractometer (Bruker Desktop D2 Phaser). The step size for the 2θ scans was 0.02° in an interval of 7°–20°.

Computational Methods. For all systems with periodic boundary conditions, DFT calculations were carried out with the Vienna ab initio simulation package (VASP),[37,38] making use of the Perdew, Burke, and Ernzerhof (PBE)[39] exchange–correlation functional based on experimentally solved crystal structures. Electron–ion interactions were described with the projector augment wave (PAW) method,[39,40] with the kinetic energy cutoff for the plane-wave basis set defined as 520 eV and a Gaussian smearing with a width of 0.05 eV employed. The convergence criterion of the total energy was set to 10^{-5} eV in the self-consistent loop. The Brillouin zone was sampled with a 4 × 4 × 4 Γ-centered grid. High-symmetry points in the first Brillouin zone used for the band structure calculations were determined with the AFLOW software,[41] which follows the scheme proposed by Setyawan and Curtarolo.[42] Carrier effective masses were calculated by performing a parabolic fitting at the region of interest in the Brillouin zone. For relatively flat bands the parabolic assumption is not valid and the finite difference result has a significant dependence on the step size used; thus, a range instead of a value is given for such flat band situations.

For systems with open boundary conditions, the geometric and electronic structures were optimized via DFT at the ωB97XD/Def2SVP level of theory[43,44] using the Gaussian 16 software suite (Revision A.03).[45] Electronic couplings for dimer models were calculated following both the energy-splitting approach and the fragment orbital approach developed by Valeev and co-workers using the code from Ryno.[46,47]

RESULTS AND DISCUSSION

In this section, we begin with a description of the dinaphtho-fused *s*-indacene-based organic semiconductors in OFETs, where widely varied OFET performance is observed as a function of the molecular chemistry and processing procedures. To develop more insight into the intrinsic performance differences, we then explore the molecular packing in bulk crystal structures and examine the electronic properties of the DNI-based materials through DFT calculations.

We begin by evaluating the electrical properties of the DNIs by incorporating them in OFETs. Since processing parameters influence film formation and film microstructure, several deposition methods and postdeposition treatments were tested for each compound to optimize the thin-film quality.[48,49] As-cast films had poor electrical performance stemming from the poor degree of order (see SI Figures S2 and S3). Exposure of an organic thin film to solvent vapors has been shown to increase film crystallinity and consequently device performance.[50] Hence, to improve the thin-film crystallinity, the as-cast films were then subjected to solvent vapor annealing. We made use of five solvents, ranging from low to high vapor pressures, with and without adding heat (75 °C). XRD spectra and images of the films pre- and postprocessing are provided in the SI; the best devices from each material are reported in the main text. These spectra also confirm that the polymorphs obtained in the crystalline thin film coincide with those in the single crystals, validating our comparison between the calculations, which are based on the single-crystal structures and the experimental results obtained in thin films.

DOI: 10.1021/acs.chemmater.9b01436
Chem. Mater. 2019, 31, 6962–6970

We begin our discussion by comparing the *linear* DNI regioisomers, which vary chemically in the alkyl chains implemented in the trialkylsilyl groups. While nODIPS spin coated films did not respond to SVA and TIBS films exhibited minor morphological changes, SVA had a notable effect on the TIPS substituted molecules. SVA-treated films of the TIPS *linear* DNI were highly crystalline (see Figures S2 and S3), with a preferential (001) out-of-plane orientation as verified by XRD; results obtained upon SVA in chlorobenzene are shown in Figure 1d,f. Notably, the diffraction pattern is consistent with that measured for bulk single crystals (see below), confirming that the crystal symmetry in the thin film is consistent with that obtained for the bulk crystal.

OFETs were fabricated in top-gate, bottom-contact configurations, using either Au or Ag source and drain contacts and a Cytop gate dielectric, as shown in Figure 2a.[36] The electrodes were fabricated following our recently developed procedure to achieve a low contact resistance.[18] Cytop provides a low trap density at the interface with semiconductors[34] and has a thermal expansion coefficient similar to those of most organic semiconductors, which will prevent the formation of microstrain-induced electronic traps.[51] In spite of our attempts to improve film quality and device architecture, the nODIPS (Figure 1a) and TIBS (Figure 1b) films did not yield working transistors. This could result from the fact that the film morphologies were not ideal or might be related to the intrinsic material properties, as we will discuss later. On the other hand, devices fabricated from TIPS *linear* DNI (Figure 1c) SVA films exhibit hole mobilities of 1.04 ± 0.68 $cm^2/(V\ s)$, with a maximum of 2.25 $cm^2/(V\ s)$ (see SI Figure S4). The mobilities were evaluated in the saturation regime.[36]

Encouraged by the performance of the TIPS *linear* DNI molecule, we analyzed the *syn* and *anti* regioisomers with the TIPS substituents (Figure 1e,g), using similar deposition methods to fabricate thin films with these isomers. Unfortunately, OFETs with a conducting channel made from TIPS *syn* DNI did not yield working devices (neither p- nor n-type channels). On the other hand, OFETs fabricated from TIPS *anti* DNI exhibit hole mobilities of 4.72 ± 1.97 $cm^2/(V\ s)$, with a maximum of 7.1 $cm^2/(V\ s)$. Importantly, these mobilities represent a considerable advance in the performance of organic semiconductors derived from antiaromatic building blocks. Panels b and c of Figure 2 present example current–voltage characteristics, with the transfer curve (the dependence of the drain current (I_D) on the gate-source voltage (V_{GS})) being shown in Figure 2b and the output curve (the dependence of I_D on the source-drain voltage (V_{DS})) in Figure 2c. High threshold voltages (V_{th}) were quite common in the OFETs fabricated from this material, which indicates high trap density at the semiconductor/dielectric interface, in spite of the fact that we used a polymer dielectric that tends to afford low trap densities at the interface of the semiconductor.[34,52,53] Other device parameters include the on/off ratio, which exceeded 10^4 in all our devices and reached values as high as 10^8. Subthreshold swings fluctuated from 1.5 to 2.5 V/decade. We further noticed that the TIPS *anti* DNI films exhibited ambipolar behavior at high positive voltages, but unfortunately we were not able to evaluate the electron mobility because a pure n-type channel was not observed (see Figure S5).

Single-crystal X-ray diffraction measurements were performed on crystals of each of the five compounds to determine the impact of the chemical structure modifications on the

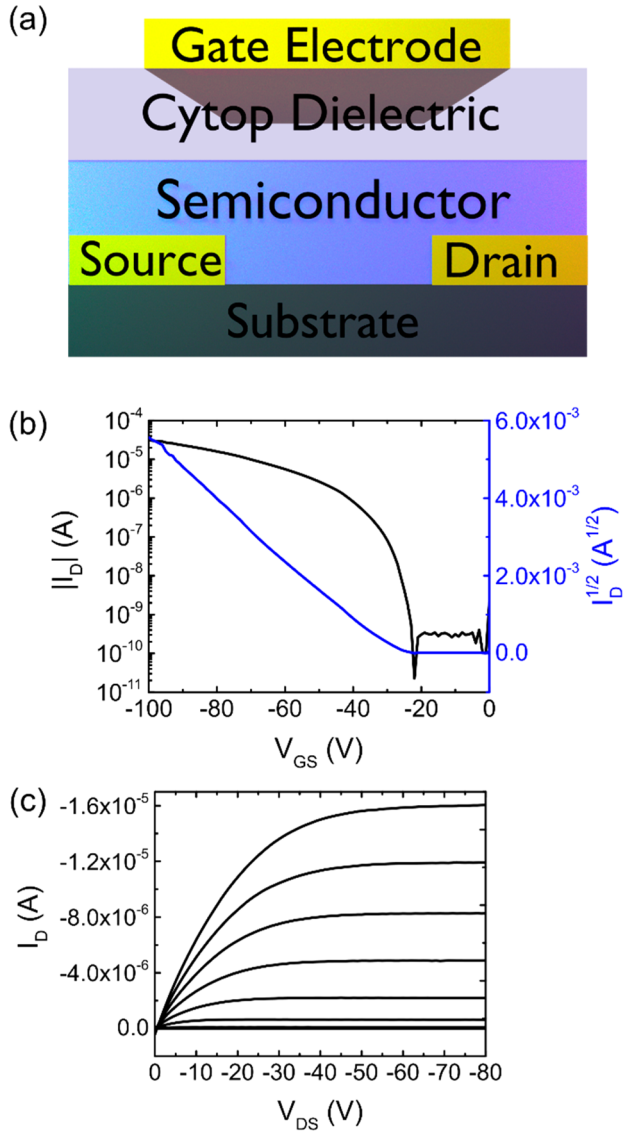

Figure 2. Device structure and electrical characteristics for TIPS *anti* DNI. (a) Top-gate, bottom-contact field-effect transistors, (b) drain current vs gate-source voltage (I_D–V_{GS}) in the saturation regime V_{DS} = −60 V, and (c) drain current vs drain-source voltage (I_D–V_{DS}) for an OFET made with TIPS *anti* DNI isomer. Each curve corresponds to a constant V_{GS}, from 0 to −60 V in −10 V steps.

crystal packing. The solid-state packing in nODIPS (Figure 3a), TIBS *linear* (Figure 3b), and TIPS *syn* (Figure 3e,f) DNIs consist of π-stacking motifs that predominantly showcase one-dimensional (1D) stacking interactions among the π-conjugated backbones. While large intermolecular electronic couplings can be a characteristic in these systems, efficient charge-carrier transport is often not expected in (crystalline) thin films derived from such packing motifs.[54] In sharp contrast, TIPS *linear* DNI (Figure 3c) and TIPS *anti* DNI (Figure 3d) both crystallize in a two-dimensional (2D) π-stacked motif, namely, a 2D brickwork pattern, which is known to lead to superior electrical properties in thin-film transistors.[14,18,53,55] The TIBS *linear*, TIPS *syn*, and TIPS *anti* derivatives follow the empirical rule established by Anthony and collaborators, which states that when the diameter of the solubilizing substituent is less than half the length of the backbone, a 1-D slipped stack packing

DOI: 10.1021/acs.chemmater.9b01436
Chem. Mater. 2019, 31, 6962–6970

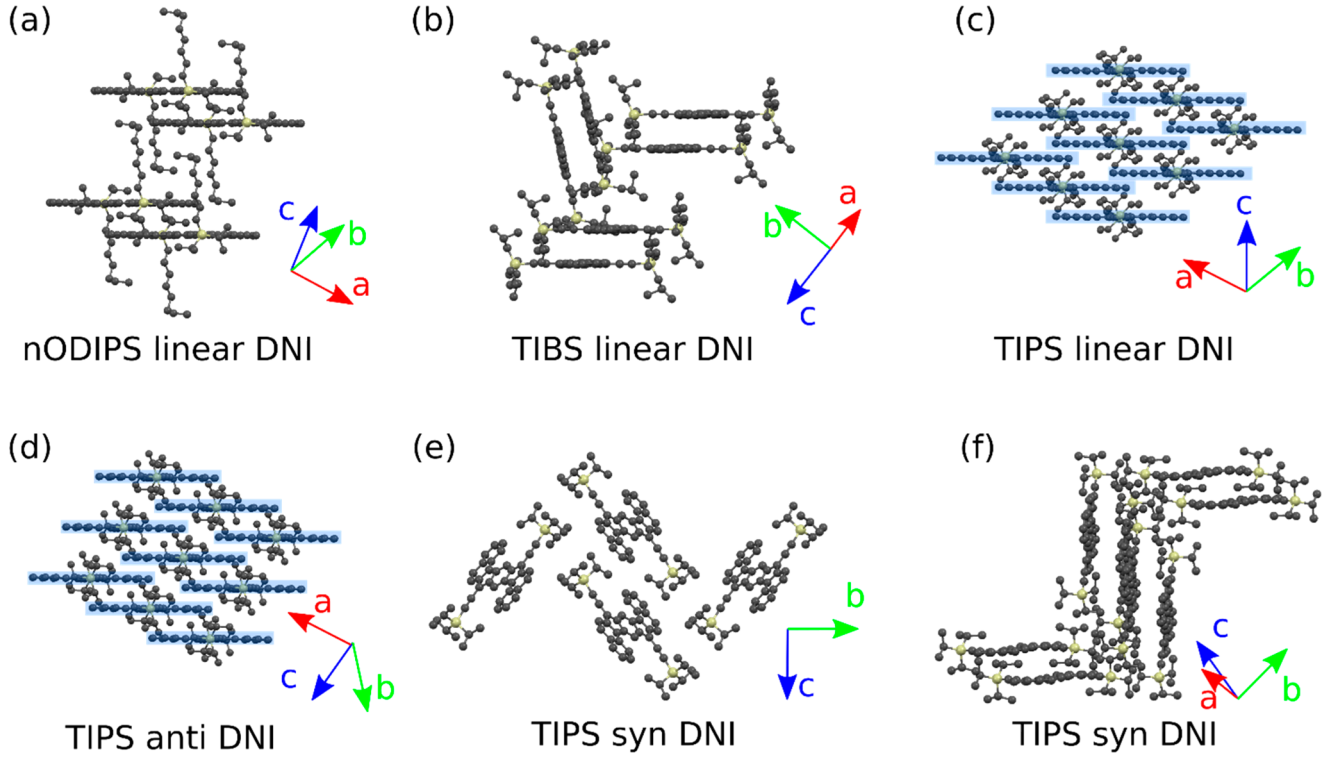

Figure 3. Solid-state packing for each DNI isomer: (a) nODIPS *linear* DNI, (b) TIBS *linear* DNI, (c) TIPS *linear* DNI, (d) TIPS *anti* DNI, (e) TIPS *syn* DNI along the *a* direction, and (f) TIPS *syn* DNI viewed down the long axis of the backbone. Note that TIPS *linear* DNI and TIPS *anti* DNI are the only two bulk crystals to exhibit a 2D brickwork packing pattern. For these molecules, the backbone was highlighted with a blue rectangle, which is a guide to the eye to allow for better illustration of the brickwork pattern.

arrangement is obtained and for larger diameters, a 2D structure is more stable.[56] nODIPS and TIPS *linear*, however, deviate from this rule, emphasizing, again how challenging it is to predict crystalline packing from molecular structures.

In organic semiconductors, the spatial overlap of the π-conjugated backbones governs in part the wave function overlap, a characteristic of importance to describe the propensity for charge-carrier transport.[54,57] To evaluate the electronic characteristics of each DNI derivative, we made use of a combination of periodic band structure calculations and the direct determination of the electronic couplings from dimer models, both in the DFT framework. A summary of the periodic DFT results is provided in Table 1, along with the experimental values obtained for the OFET-extracted hole mobilities, and select electronic band structures are shown in Figure 4; note that the periodic DFT calculations provide a representation of the idealized case of charge-carrier transport through the bulk of a crystal. For both the TIBS and nODIPS *linear* DNI, the valence and conduction bands are relatively flat, which result in charge carriers with large effective masses. These results correlate with the small spatial overlap of the π-conjugated backbones found in the experimental crystal structures and are consistent with the limited OFET performance.

Table 1. DFT-Derived Electron Effective Mass (m_e), Hole Effective Mass (m_h), and Experimentally Measured Hole Mobilites (μ_h)

crystal	μ_h (cm^2/(V s))	m_e (m_0)	m_h (m_0)
nODIPS *linear* DNI		3.53−4.97[a]	3.42−3.94[a]
TIBS *linear* DNI		2.19	5.21−6.36[a]
TIPS *linear* DNI	1.04 ± 0.68	1.78	3.57
TIPS *syn* DNI		1.63	0.85
TIPS *anti* DNI	4.72 ± 1.97	0.39	0.52

[a]The effective mass calculation assumes that the dispersion relation is parabolic at the zone edge. If this relation deviates severely from that of a parabola (e.g., the band is flat), the numerical fitting will give a range rather than a point.

The periodic DFT calculations for the TIPS-substituted regioisomers suggest that both the *syn* and *anti* isomers should have superior electronic characteristics when compared to the *linear* isomer (Figure 4, Table 1), as a larger hole effective mass and less dispersive valence and conduction bands are obtained for the latter. This finding is satisfied when one compares the OFET performance of the *anti* and *linear* isomers. The *syn* isomer, however, has a 1D slipped-stack packing structure, and hence it is not unusual that the material performance was poor in the OFET testing.[58]

Interestingly, for TIPS *linear* DNI, the periodic DFT calculations indicate the existence of fairly heavy holes, on the order of those determined for the nODIPS *linear* DNI, which would suggest limited charge transport characteristics. Nevertheless, OFETs consistently yield mobilities on the order of 1 cm^2/(V s). Though the backbone overlap of the TIPS *linear* DNI is relatively large, the HOMO−HOMO coupling ~ 7 meV for a dimer model extracted from the bulk crystal is quite small. We recall here that it is the wave function overlap, and not necessarily the spatial overlap of the π-conjugated backbones, that is a critical metric for evaluating the potential for a material to perform well in OFET applications. Given the discrepancy between reasonable OFET performance and small intermolecular electronic coupling/large hole effective mass for

DOI: 10.1021/acs.chemmater.9b01436
Chem. Mater. 2019, 31, 6962−6970

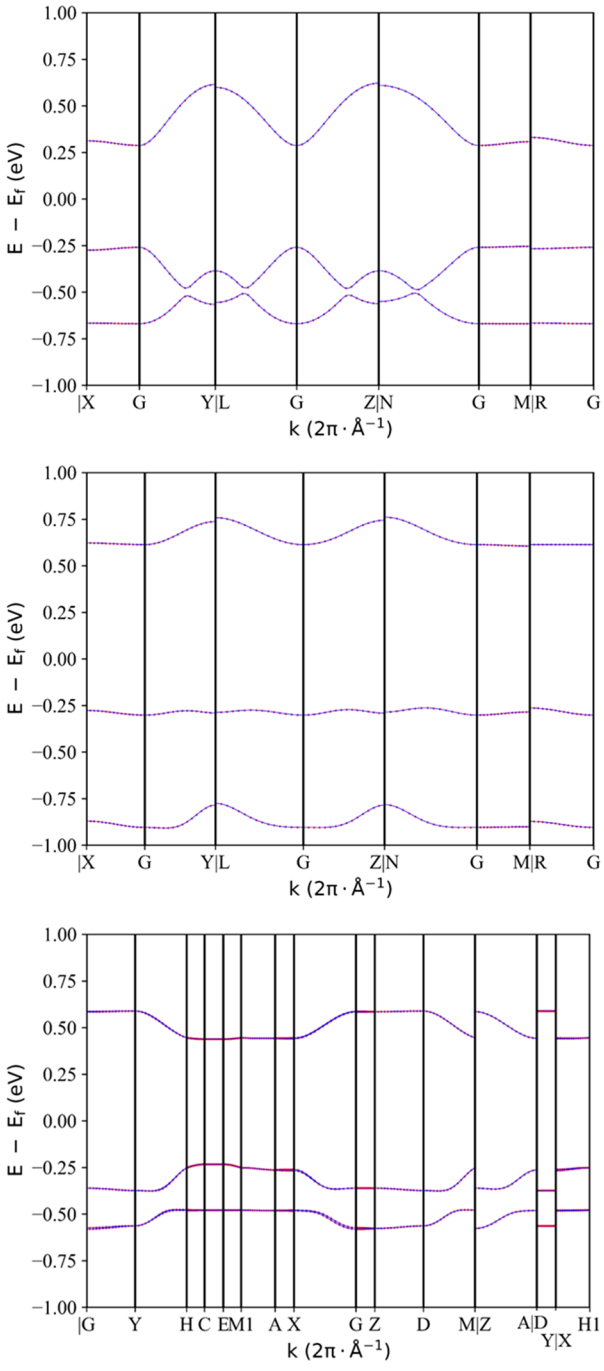

Figure 4. Electronic band structures for (from top to bottom) TIPS *anti* DNI, TIPS *syn* DNI, and TIPS *linear* DNI, where the energies are shifted such that the Fermi level is at 0.00 eV.

TIPS *linear* DNI, we suspect that the static picture, which sets the framework for this evaluation and includes neither molecular nor lattice dynamics, may not be sufficient to describe the behavior of TIPS *linear* DNI; i.e., it is well-established that electron−phonon couplings can play indispensable roles in the charge-carrier transport characteristics of organic semiconductors.[54,59−61] As a first-order approximation to such effects in TIPS *linear* DNI, we inspected the HOMO−HOMO electronic couplings as a function of in-plane intermolecular translations within a dimer model (Figure 5): The interbackbone distance is fixed at 3.45 Å, as extracted from the crystal structure, with the monomer geometry being that

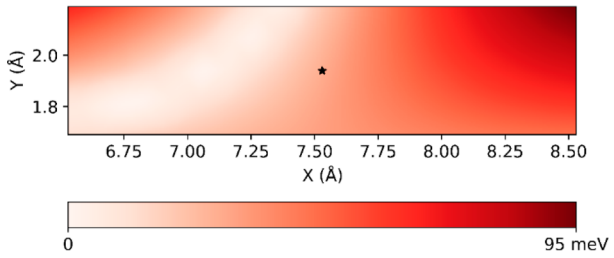

Figure 5. Electronic couplings as a function of intermolecular slip in a dimer model. *X* and *Y* indicate long and short axis slips, respectively. The black star indicates the slips calculated from crystal structure in TIPS *linear* DNI.

optimized at the ωB97XD/Def2SVP level of theory. Effectively, translation among points on the map of intermolecular coupling as a function of backbone displacement can be used as an estimate to expected effects related to intermolecular phonon modes. We note that the intermolecular displacements in organic semiconductors can be relatively large, of the order of 0.5 Å in the related TIPS-pentacene molecular material, which are a function of the relatively weak, noncovalent interactions among the molecules in the solid state.[62−64] Specifically for TIPS *linear* DNI, sub-angstrom translations can lead to significant increases in the electronic couplings, and hence it would not be surprising that select lattice phonons could lead to enhanced electronic couplings that would improve the charge-carrier transport behavior when compared to the description derived from a static representation. Further, we note that at identical intermolecular positions, the electronic coupling for a dimer built from DFT-optimized monomer geometries (∼35 meV) is larger than the counterpart dimer with the geometries extracted directly from the crystal structure (∼7 meV). This result suggests that modest intramolecular geometry changes can also lead to notable changes in the intermolecular electronic couplings. The combination of the large changes in the intermolecular electronic couplings as a function of molecular displacement and changes in molecular geometry suggest that the static DFT picture may be inadequate to appropriately describe the transport characteristics of TIPS *linear* DNI; future work on these materials will include direct evaluations of the electron−phonon couplings to confirm this hypothesis.

Finally, we note that we were not able to measure electron transport, despite the small effective mass calculated for electrons, in any of these systems. These results are, perhaps, due in part to inadequate choice of electrode materials, and/or trapping at the interface with the dielectric, which is more prevalent for the electrons than for holes.[36,65] Note that here we limited our analysis to the evaluation of the impact of substitution on the packing motif and electronic couplings, while ignoring the shifts introduced in the molecule's ionization potential and electron affinity. Such shifts can be substantial and can lead to inefficient charge injection in the case of large injection barriers between the semiconductor and the device electrode.

■ CONCLUSION

In summary, we synthesized a series of dinaphtho-fused *s*-indacenes where we varied both the chemistry of the (trialkylsilyl)ethynyl-substituents and the backbone geometries and characterized the charge-carrier transport properties. We found that the TIBS and nODIPS substituents on the

DOI: 10.1021/acs.chemmater.9b01436
Chem. Mater. 2019, 31, 6962−6970

linear DNI framework promote a predominantly 1D-packing motif, which results in films with poor electrical performance, in agreement with the outcome from the periodic DFT band structure calculations. The TIPS functional group, on the other hand, yielded a 2D bricklayer packing and hole mobilities of 1.04 ± 0.68 $cm^2/(V\ s)$ in the *linear* DNI. Hole mobilities exceeding 7 $cm^2/(V\ s)$ and a weak signature of ambipolar transport were found in TIPS *anti* DNI. Conversely, we were unable to achieve working devices from the TIPS *syn* DNI isomer, despite low effective masses predicted for both electrons and holes calculated for this compound, a typical result encountered for materials that take on a 1D slipped-stack packing configuration. Our results demonstrate that reducing molecule aromaticity while preserving the conjugation length represents an efficient tool for achieving favorable charge transport, but fine-tuning the chemistry is critical. Manipulating the molecular structure to generate predictable changes to the crystalline packing remains a challenge in crystal engineering given the weak nature of the intermolecular interactions characteristic to organic solids.

■ ASSOCIATED CONTENT

Supporting Information

The Supporting Information is available free of charge on the ACS Publications website at DOI: 10.1021/acs.chemmater.9b01436.

Preparation details and NMR spectra of nODIPS *linear* DNI, X-ray diffraction of nODIPS, TIBS, and TIPS *linear* DNI, optical micrographs illustrating the effect of solvent annealing on nODIPS, TIBS, and TIPS *linear* DNI, electrical characteristics of TIPS *linear* DNI field-effect transistors, and electrical measurements exhibiting ambipolar signature in TIPS *anti* DNI (PDF)

■ AUTHOR INFORMATION

Corresponding Author

*E-mail: jurchescu@wfu.edu.

ORCID

Conerd K. Frederickson: 0000-0002-1194-7908
Chad Risko: 0000-0001-9838-5233
Michael M. Haley: 0000-0002-7027-4141
Oana D. Jurchescu: 0000-0003-2204-2909

Notes

The authors declare no competing financial interest.

■ ACKNOWLEDGMENTS

The device and the theory work were supported by the National Science Foundation Designing Materials to Revolutionize and Engineer our Future (NSF DMREF) program under Awards DMR-1627925 and DMR-1627428, respectively. The synthetic work was supported by the NSF (Grant CHE-1565780). Supercomputing resources on the Lipscomb High Performance Computing Cluster were provided by the University of Kentucky Information Technology Department and Center for Computational Sciences (CCS). Mass spectrometry capabilities in the CAMCOR facility at Oregon are supported by NSF Grant CHE-1625529. XRD measurements of thin films were performed at Wake Forest University with assistance from Dr. Cynthia Day.

■ REFERENCES

(1) Abdellah, A.; Fabel, B.; Lugli, P.; Scarpa, G. Spray Deposition of Organic Semiconducting Thin-Films: Towards the Fabrication of Arbitrary Shaped Organic Electronic Devices. *Org. Electron.* **2010**, *11* (6), 1031−1038.

(2) Sirringhaus, H.; Kawase, T.; Friend, R. H.; Shimoda, T.; Inbasekaran, M.; Wu, W.; Woo, E. P. High-Resolution Inkjet Printing of All-Polymer Transistor Circuits. *Science* **2000**, *290* (5499), 2123−2126.

(3) Sekitani, T.; Noguchi, Y.; Zschieschang, U.; Klauk, H.; Someya, T. Organic Transistors Manufactured Using Inkjet Technology with Subfemtoliter Accuracy. *Proc. Natl. Acad. Sci. U. S. A.* **2008**, *105* (13), 4976−4980.

(4) Diemer, P. J.; Harper, A. F.; Niazi, M. R.; Petty, A. J.; Anthony, J. E.; Amassian, A.; Jurchescu, O. D. Laser-Printed Organic Thin-Film Transistors. *Adv. Mater. Technol.* **2017**, *2* (11), 1700167.

(5) Lin, Y.-Y.; Gundlach, D. I.; Nelson, S. F.; Jackson, T. N. Pentacene-Based Organic Thin-Film Transistors. *IEEE Trans. Electron Devices* **1997**, *44* (8), 1325−1331.

(6) Jurchescu, O. D.; Popinciuc, M.; van Wees, B. J.; Palstra, T. T. M. Interface-Controlled, High-Mobility Organic Transistors. *Adv. Mater.* **2007**, *19* (5), 688−692.

(7) de Boer, R. W. I.; Klapwijk, T. M.; Morpurgo, A. F. Field-Effect Transistors on Tetracene Single Crystals. *Appl. Phys. Lett.* **2003**, *83* (21), 4345−4347.

(8) Podzorov, V.; Sysoev, S. E.; Loginova, E.; Pudalov, V. M.; Gershenson, M. E. Single-Crystal Organic Field Effect Transistors with the Hole Mobility ∼8 cm2/V s. *Appl. Phys. Lett.* **2003**, *83* (17), 3504−3506.

(9) Anthony, J. E. Functionalized Acenes and Heteroacenes for Organic Electronics. *Chem. Rev.* **2006**, *106* (12), 5028−5048.

(10) Fudickar, W.; Linker, T. Why Triple Bonds Protect Acenes from Oxidation and Decomposition. *J. Am. Chem. Soc.* **2012**, *134* (36), 15071−15082.

(11) Zade, S. S.; Zamoshchik, N.; Reddy, A. R.; Fridman-Marueli, G.; Sheberla, D.; Bendikov, M. Products and Mechanism of Acene Dimerization. A Computational Study. *J. Am. Chem. Soc.* **2011**, *133* (28), 10803−10816.

(12) Schleyer, P. v. R.; Manoharan, M.; Jiao, H.; Stahl, F. The Acenes: Is There a Relationship between Aromatic Stabilization and Reactivity? *Org. Lett.* **2001**, *3* (23), 3643−3646.

(13) Goetz, K. P.; Li, Z.; Ward, J. W.; Bougher, C.; Rivnay, J.; Smith, J.; Conrad, B. R.; Parkin, S. R.; Anthopoulos, T. D.; Salleo, A.; Anthony, J. E.; Jurchescu, O. D. Effect of Acene Length on Electronic Properties in 5-, 6-, and 7-Ringed Heteroacenes. *Adv. Mater.* **2011**, *23* (32), 3698−3703.

(14) Subramanian, S.; Park, S. K.; Parkin, S. R.; Podzorov, V.; Jackson, T. N.; Anthony, J. E. Chromophore Fluorination Enhances Crystallization and Stability of Soluble Anthradithiophene Semiconductors. *J. Am. Chem. Soc.* **2008**, *130* (9), 2706−2707.

(15) Niimi, K.; Kang, M. J.; Miyazaki, E.; Osaka, I.; Takimiya, K. General Synthesis of Dinaphtho[2,3- *b*:2′,3′- *f*]Thieno[3,2- *b*]Thiophene (DNTT) Derivatives. *Org. Lett.* **2011**, *13* (13), 3430−3433.

(16) Huckaba, A. J.; Giordano, F.; McNamara, L. E.; Dreux, K. M.; Hammer, N. I.; Tschumper, G. S.; Zakeeruddin, S. M.; Grätzel, M.; Nazeeruddin, M. K.; Delcamp, J. H. Indolizine-Based Donors as Organic Sensitizer Components for Dye-Sensitized Solar Cells. *Adv. Energy Mater.* **2015**, *5* (7), 1401629.

(17) Granger, D. B.; Mei, Y.; Thorley, K. J.; Parkin, S. R.; Jurchescu, O. D.; Anthony, J. E. Synthesis and Electrical Properties of Derivatives of 1,4-Bis(Trialkylsilylethynyl)Benzo[2,3- B:5,6- b ′]Diindolizines. *Org. Lett.* **2016**, *18* (23), 6050−6053.

(18) Lamport, Z. A.; Barth, K. J.; Lee, H.; Gann, E.; Engmann, S.; Chen, H.; Guthold, M.; McCulloch, I.; Anthony, J. E.; Richter, L. J.; DeLongchamp, D. M.; Jurchescu, O. D. A Simple and Robust Approach to Reducing Contact Resistance in Organic Transistors. *Nat. Commun.* **2018**, *9* (1), 5130.

DOI: 10.1021/acs.chemmater.9b01436
Chem. Mater. 2019, 31, 6962−6970

(19) Yuan, Y.; Giri, G.; Ayzner, A. L.; Zoombelt, A. P.; Mannsfeld, S. C. B.; Chen, J.; Nordlund, D.; Toney, M. F.; Huang, J.; Bao, Z. Ultra-High Mobility Transparent Organic Thin Film Transistors Grown by an off-Centre Spin-Coating Method. *Nat. Commun.* **2014**, *5*, 3005.
(20) Rudebusch, G. E.; Haley, M. M. In *Polycyclic Arenes and Heteroarenes*; Miao, Q., Ed.; Wiley-VCH Verlag: Weinheim, Germany, 2015; pp 37−60, DOI: 10.1002/9783527689545.ch2.
(21) Minsky, A.; Meyer, A. Y.; Rabinovitz, M. Paratropicity and Antiaromaticity: Role of the Homo-Lumo Energy Gap. *Tetrahedron* **1985**, *41* (4), 785−791.
(22) Frederickson, C. K.; Rose, B. D.; Haley, M. M. Explorations of the Indenofluorenes and Expanded Quinoidal Analogues. *Acc. Chem. Res.* **2017**, *50* (4), 977−987.
(23) London, G.; von Wantoch Rekowski, M.; Dumele, O.; Schweizer, W. B.; Gisselbrecht, J.-P.; Boudon, C.; Diederich, F. Pentalenes with Novel Topologies: Exploiting the Cascade Carbopalladation Reaction between Alkynes and Gem-Dibromoolefins. *Chem. Sci.* **2014**, *5* (3), 965−972.
(24) Marshall, J. L.; Uchida, K.; Frederickson, C. K.; Schütt, C.; Zeidell, A. M.; Goetz, K. P.; Finn, T. W.; Jarolimek, K.; Zakharov, L. N.; Risko, C.; Herges, R.; Jurchescu, O. D.; Haley, M. M.; et al. Indacenodibenzothiophenes: Synthesis, Optoelectronic Properties and Materials Applications of Molecules with Strong Antiaromatic Character. *Chem. Sci.* **2016**, *7* (8), 5547−5558.
(25) Frederickson, C. K.; Zakharov, L. N.; Haley, M. M. Modulating Paratropicity Strength in Diareno-Fused Antiaromatics. *J. Am. Chem. Soc.* **2016**, *138* (51), 16827−16838.
(26) Jin, Z.; Teo, Y. C.; Zulaybar, N. G.; Smith, M. D.; Xia, Y. Streamlined Synthesis of Polycyclic Conjugated Hydrocarbons Containing Cyclobutadienoids via C−H Activated Annulation and Aromatization. *J. Am. Chem. Soc.* **2017**, *139* (5), 1806−1809.
(27) Kawase, T.; Fujiwara, T.; Kitamura, C.; Konishi, A.; Hirao, Y.; Matsumoto, K.; Kurata, H.; Kubo, T.; Shinamura, S.; Mori, H.; et al. Dinaphthopentalenes: Pentalene Derivatives for Organic Thin-Film Transistors. *Angew. Chem., Int. Ed.* **2010**, *49* (42), 7728−7732.
(28) Konishi, A.; Fujiwara, T.; Ogawa, N.; Hirao, Y.; Matsumoto, K.; Kurata, H.; Kubo, T.; Kitamura, C.; Kawase, T. Pentaleno[1,2- *c*:4,5- *c* ′]Dithiophene Derivatives: First Synthesis, Properties, and a Molecular Structure. *Chem. Lett.* **2010**, *39* (3), 300−301.
(29) Naibi Lakshminarayana, A.; Chang, J.; Luo, J.; Zheng, B.; Huang, K.-W.; Chi, C. Bisindeno-Annulated Pentacenes with Exceptionally High Photo-Stability and Ordered Molecular Packing: Simple Synthesis by a Regio-Selective Scholl Reaction. *Chem. Commun.* **2015**, *51* (17), 3604−3607.
(30) Chase, D. T.; Fix, A. G.; Kang, S. J.; Rose, B. D.; Weber, C. D.; Zhong, Y.; Zakharov, L. N.; Lonergan, M. C.; Nuckolls, C.; Haley, M. M. 6,12-Diarylindeno[1,2-b]Fluorenes: Syntheses, Photophysics, and Ambipolar OFETs. *J. Am. Chem. Soc.* **2012**, *134* (25), 10349−10352.
(31) Jin, Z.; Yao, Z.-F.; Barker, K. P.; Pei, J.; Xia, Y. Dinaphthobenzo[1,2:4,5]Dicyclobutadiene: Antiaromatic and Orthogonally Tunable Electronics and Packing. *Angew. Chem., Int. Ed.* **2019**, *58* (7), 2034−2039.
(32) Wang, J.; Chu, M.; Fan, J.-X.; Lau, T.-K.; Ren, A.-M.; Lu, X.; Miao, Q. Crystal Engineering of Biphenylene-Containing Acenes for High-Mobility Organic Semiconductors. *J. Am. Chem. Soc.* **2019**, *141* (8), 3589−3596.
(33) Barker, J. E.; Kodama, T.; Song, M. K.; Frederickson, C. K.; Jousselin-Oba, T.; Zakharov, L. N.; Marrot, J.; Frigoli, M.; Johnson, R. P.; Haley, M. M. Serendipitous Rediscovery of the Facile Cyclization of Z,Z-3,5-Octadiene-1,7-diyne Derivatives to Afford Stable, Substituted Naphthocyclobutadienes. *ChemPlusChem* **2019**, *84*, DOI: 10.1002/cplu.201800605.
(34) Diemer, P. J.; Lamport, Z. A.; Mei, Y.; Ward, J. W.; Goetz, K. P.; Li, W.; Payne, M. M.; Guthold, M.; Anthony, J. E.; Jurchescu, O. D. Quantitative Analysis of the Density of Trap States at the Semiconductor-Dielectric Interface in Organic Field-Effect Transistors. *Appl. Phys. Lett.* **2015**, *107* (10), 103303.
(35) Ward, J. W.; Loth, M. A.; Kline, R. J.; Coll, M.; Ocal, C.; Anthony, J. E.; Jurchescu, O. D. Tailored Interfaces for Self-Patterning Organic Thin-Film Transistors. *J. Mater. Chem.* **2012**, *22* (36), 19047−19053.
(36) Lamport, Z. A.; Haneef, H. F.; Anand, S.; Waldrip, M.; Jurchescu, O. D. Tutorial: Organic Field-Effect Transistors: Materials, Structure and Operation. *J. Appl. Phys.* **2018**, *124* (7), No. 071101.
(37) Kresse, G.; Furthmüller, J. Efficient Iterative Schemes for Ab Initio Total-Energy Calculations Using a Plane-Wave Basis Set. *Phys. Rev. B: Condens. Matter Mater. Phys.* **1996**, *54* (16), 11169−11186.
(38) Kresse, G.; Furthmüller, J. Efficiency of Ab-Initio Total Energy Calculations for Metals and Semiconductors Using a Plane-Wave Basis Set. *Comput. Mater. Sci.* **1996**, *6* (1), 15−50.
(39) Perdew, J. P.; Chevary, J. A.; Vosko, S. H.; Jackson, K. A.; Pederson, M. R.; Singh, D. J.; Fiolhais, C. Atoms, Molecules, Solids, and Surfaces: Applications of the Generalized Gradient Approximation for Exchange and Correlation. *Phys. Rev. B: Condens. Matter Mater. Phys.* **1992**, *46* (11), 6671−6687.
(40) Kresse, G.; Joubert, D. From Ultrasoft Pseudopotentials to the Projector Augmented-Wave Method. *Phys. Rev. B: Condens. Matter Mater. Phys.* **1999**, *59* (3), 1758−1775.
(41) Curtarolo, S.; Setyawan, W.; Hart, G. L. W.; Jahnatek, M.; Chepulskii, R. V.; Taylor, R. H.; Wang, S.; Xue, J.; Yang, K.; Levy, O.; et al. AFLOW: An Automatic Framework for High-Throughput Materials Discovery. *Comput. Mater. Sci.* **2012**, *58*, 218−226.
(42) Setyawan, W.; Curtarolo, S. High-Throughput Electronic Band Structure Calculations: Challenges and Tools. *Comput. Mater. Sci.* **2010**, *49* (2), 299−312.
(43) Weigend, F.; Ahlrichs, R. Balanced Basis Sets of Split Valence, Triple Zeta Valence and Quadruple Zeta Valence Quality for H to Rn: Design and Assessment of Accuracy. *Phys. Chem. Chem. Phys.* **2005**, *7* (18), 3297.
(44) Chai, J.-D.; Head-Gordon, M. Long-Range Corrected Hybrid Density Functionals with Damped Atom−atom Dispersion Corrections. *Phys. Chem. Chem. Phys.* **2008**, *10* (44), 6615.
(45) Frisch, M. J.; Trucks, G. W.; Schlegel, H. B.; Scuseria, G. E.; Robb, M. A.; Cheeseman, J. R.; Scalmani, G.; Barone, V.; Petersson, G. A.; Nakatsuji, H.; et al. *Gaussian 16*, Revision B.01; Gaussian: Wallingford, CT, USA, 2016.
(46) Ryno, S. Transfer Integral Calculator, 2017.
(47) Valeev, E. F.; Coropceanu, V.; da Silva Filho, D. A.; Salman, S.; Brédas, J.-L. Effect of Electronic Polarization on Charge-Transport Parameters in Molecular Organic Semiconductors. *J. Am. Chem. Soc.* **2006**, *128* (30), 9882−9886.
(48) DeLongchamp, D. M.; Vogel, B. M.; Jung, Y.; Gurau, M. C.; Richter, C. A.; Kirillov, O. A.; Obrzut, J.; Fischer, D. A.; Sambasivan, S.; Richter, L. J.; et al. Variations in Semiconducting Polymer Microstructure and Hole Mobility with Spin-Coating Speed. *Chem. Mater.* **2005**, *17* (23), 5610−5612.
(49) Chen, J.; Shao, M.; Xiao, K.; Rondinone, A. J.; Loo, Y. L.; Kent, P. R. C.; Sumpter, B. G.; Li, D.; Keum, J. K.; Diemer, P. J.; et al. Solvent-Type-Dependent Polymorphism and Charge Transport in a Long Fused-Ring Organic Semiconductor. *Nanoscale* **2014**, *6* (1), 449−456.
(50) Dickey, K. C.; Anthony, J. E.; Loo, Y. L. Improving Organic Thin-Film Transistor Performance through Solvent-Vapor Annealing of Solution-Processable Triethylsilylethynyl Anthradithiophene. *Adv. Mater.* **2006**, *18* (13), 1721−1726.
(51) Mei, Y.; Diemer, P. J.; Niazi, M. R.; Hallani, R. K.; Jarolimek, K.; Day, C. S.; Risko, C.; Anthony, J. E.; Amassian, A.; Jurchescu, O. D. Crossover from Band-like to Thermally Activated Charge Transport in Organic Transistors Due to Strain-Induced Traps. *Proc. Natl. Acad. Sci. U. S. A.* **2017**, *114* (33), E6739−E6748.
(52) Jia, X.; Fuentes-Hernandez, C.; Wang, C.; Park, Y.; Kippelen, B. Stable Organic Thin-Film Transistors. *Sci. Adv.* **2018**, *4* (1), eaao1705.
(53) Stevens, L. A.; Goetz, K. P.; Fonari, A.; Shu, Y.; Williamson, R. M.; Brédas, J.-L.; Coropceanu, V.; Jurchescu, O. D.; Collis, G. E. Temperature-Mediated Polymorphism in Molecular Crystals: The Impact on Crystal Packing and Charge Transport. *Chem. Mater.* **2015**, *27* (1), 112−118.

DOI: 10.1021/acs.chemmater.9b01436
Chem. Mater. 2019, 31, 6962−6970

(54) Coropceanu, V.; Cornil, J.; da Silva Filho, D. A.; Olivier, Y.; Silbey, R.; Brédas, J.-L. Charge Transport in Organic Semiconductors. *Chem. Rev.* **2007**, *107* (4), 926−952.
(55) Jurchescu, O. D.; Subramanian, S.; Kline, R. J.; Hudson, S. D.; Anthony, J. E.; Jackson, T. N.; Gundlach, D. J. Organic Single-Crystal Field-Effect Transistors of a Soluble Anthradithiophene. *Chem. Mater.* **2008**, *20* (21), 6733−6737.
(56) Anthony, J. E.; Eaton, D. L.; Parkin, S. R. A Road Map to Stable, Soluble, Easily Crystallized Pentacene Derivatives. *Org. Lett.* **2002**, *4* (1), 15−18.
(57) Bredas, J. L.; Calbert, J. P.; da Silva Filho, D. A.; Cornil, J. Organic Semiconductors: A Theoretical Characterization of the Basic Parameters Governing Charge Transport. *Proc. Natl. Acad. Sci. U. S. A.* **2002**, *99* (9), 5804−5809.
(58) Würthner, F.; Schmidt, R. Electronic and Crystal Engineering of Acenes for Solution-Processible Self-Assembling Organic Semiconductors. *ChemPhysChem* **2006**, *7* (4), 793−797.
(59) Xie, X.; Santana-Bonilla, A.; Troisi, A. Nonlocal Electron−Phonon Coupling in Prototypical Molecular Semiconductors from First Principles. *J. Chem. Theory Comput.* **2018**, *14* (7), 3752−3762.
(60) Vermeulen, D.; Corbin, N.; Goetz, K. P.; Jurchescu, O. D.; Coropceanu, V.; McNeil, L. E. Electron-Phonon Coupling in Anthracene-Pyromellitic Dianhydride. *J. Chem. Phys.* **2017**, *146* (21), 214705.
(61) Li, Y.; Yi, Y.; Coropceanu, V.; Brédas, J.-L. Symmetry Effects on Nonlocal Electron-Phonon Coupling in Organic Semiconductors. *Phys. Rev. B: Condens. Matter Mater. Phys.* **2012**, *85* (24), 245201.
(62) Eggeman, A. S.; Illig, S.; Troisi, A.; Sirringhaus, H.; Midgley, P. A. Measurement of Molecular Motion in Organic Semiconductors by Thermal Diffuse Electron Scattering. *Nat. Mater.* **2013**, *12* (11), 1045−1049.
(63) Harrelson, T. F.; Dantanarayana, V.; Xie, X.; Koshnick, C.; Nai, D.; Fair, R.; Nuñez, S. A.; Thomas, A. K.; Murrey, T. L.; Hickner, M. A.; et al. Direct Probe of the Nuclear Modes Limiting Charge Mobility in Molecular Semiconductors. *Mater. Horiz.* **2019**, *6* (1), 182−191.
(64) Troisi, A.; Orlandi, G.; Anthony, J. E. Electronic Interactions and Thermal Disorder in Molecular Crystals Containing Cofacial Pentacene Units. *Chem. Mater.* **2005**, *17* (20), 5024−5031.
(65) Chua, L.-L.; Zaumseil, J.; Chang, J.-F.; Ou, E. C.-W.; Ho, P. K.-H.; Sirringhaus, H.; Friend, R. H. General Observation of -Type Field-Effect Behavior in Organic Semiconductors. *Nature* **2005**, *434* (March), 194−199.

DOI: 10.1021/acs.chemmater.9b01436
Chem. Mater. 2019, 31, 6962−6970